

# The Influence of Structural Defect on Mechanical Properties and Fracture Behaviors of Carbon Nanotubes

Hsien-Chie Cheng<sup>1</sup>, Yu-Chen Hsu<sup>2</sup> and Wen-Hwa Chen<sup>2</sup>

**Abstract:** Due to the limitation of fabrication technologies nowadays, structural or atomistic defects are often perceived in carbon nanotubes (CNTs) during the manufacturing process. The main goal of the study aims at providing a systematic investigation of the effects of atomistic defects on the nanomechanical properties and fracture behaviors of single-walled CNTs (SWCNTs) using molecular dynamics (MD) simulation. Furthermore, the correlation between local stress distribution and fracture evolution is studied. Key parameters and factors under investigation include the number, type (namely the vacancy and Stone-Wales defects), location and distribution of defects. Results show that the nanomechanical properties of the CNTs, such as the elastic modulus, ultimate strength and ultimate strain, are greatly affected by the defects and also their percentage and type. It is also found that the CNTs present a brittle fracture as the strain attains a critical value, and in addition, the fracture crack tends to propagate along the high tensile stress concentration area. Moreover, the distribution pattern of defects is another driving factor affecting the nanomechanical properties of the CNTs and the associated fracture evolutions.

**Keywords:** Molecular Dynamics, Carbon Nanotube, Nanomechanical Property, Atomistic Defect, Crack Propagation, Fracture Evolution

## 1 Introduction

Over the last decade, extensive researches on the physical characteristics of CNTs, particularly their nanomechanical properties, have been extensively carried out by way of various advanced measurement tools and nano-manipulation techniques. For example, Treacy, Ebbesen and Gibson (1996) estimated the Young's modulus of cantilevered multi-walled CNTs (MWCNTs) subjected to thermal vibration based on the free-end amplitude measured by transmission electron microscope

---

<sup>1</sup> Department of Aerospace and Systems Engineering, Feng Chia University, Taichung, Taiwan.

<sup>2</sup> Department of Power Mechanical Engineering, National Tsing Hua University, Hsinchu, Taiwan.

(TEM), and reported a wide range of 0.4-3.7 TPa. Poncharal, Wang, Ugarte and de Heer Popov (1999) derived the effective elastic modulus of CNTs in a great range from 0.1 TPa to 1 TPa through the induced electromechanical resonances. By using an atomic force microscope (AFM), Salvétat, Briggs, Bonard, Bacsa, Kulik, Stockli, Burnham and Forro (1999) measured the elastic modulus of SWCNT ropes varying from 0.6 TPa to 1.3 TPa. Yu, Lourie, Dyer, Moloni, Kelly and Ruoff (2000) conducted the measurement of the Young's modulus of MWCNTs through the tensile-loading experiment with a scanning electron microscope (SEM) as well as an AFM, and found a range from 0.27 TPa to 0.95 TPa. Demczyk, Wang, Cumings, Hetman, Han, Zettl and Ritchie (2002) conducted bending tests on individual CNTs in-situ in a TEM, and measured the Young's modulus ranging from 0.8 TPa to 0.9 TPa. In summary, the above literature review suggests that there is a great difference in the measured Young's modulus of CNTs.

Nowadays, computational approaches are becoming an increasingly crucial and powerful tool in studying nanomechanics of nanomaterials because of the development of advanced computer technologies, both hardware and software. As compared to experiment methods, they are considered more cost-effective and efficient, and thus are extensively applied in the design and analysis of nanomaterials. In literature, the most widely adopted computational techniques for exploring nanomechanics of CNTs comprise MD and multi-temporal and spatial scale simulations [Shen and Atluri (2004a); Xie and Long (2006); Xie, Han and Long (2007); Chakrabarty and Cagin (2008); Ghanbari and Naghdabadi (2009)]. For instance, Lu (1997) reported the Young's modulus of S/MWCNTs in a very limited range of 0.971-0.975 TPa based on an empirical force-constant model. Using a nonorthogonal tight-binding formalism, Hernandez, Goze, Bernier and Rubio (1998) derived the Young's modulus of SWCNTs within a confined range from 1.22 TPa to 1.26 TPa. Li and Chou (2003) found the Young's modulus of S/MWCNTs ranging from 1.0-1.1 TPa by means of a molecular structural mechanics approach. According to these literature data, the reported Young's moduli of CNTs are about 1 TPa in average.

A close comparison of the theoretical predictions with the above experimental results or even the experimental data themselves suggests an apparent disagreement. In addition, the degree of discrepancy among the experimental data tends to be more significant than that of the theoretical results. The potential causes of the difference include not only the variation of the size and chirality of CNTs and the applied measurement methods but also the structural defects in CNTs. According to literature, structural defects are often perceived during the chemical treatment and fabrication process due to the limitation of present fabrication technology. Ebbesen and Takada (1995) observed that topological defects (the Stone-Wales defects)

and incomplete bonding defects (the vacancy defects) commonly exist in CNTs. Hahn, Kang, Song and Jeon (1996) found atomistic vacancy on the graphite surface through both a scanning tunneling microscope (STM) and AFM. Besides, atomistic defects are often observed at the stage of CNT growth [Andrews, Jacques, Qian and Dickey (2001)] and purification [Mawhinney, Naumenko, Kuznetsova, Yates Jr., Liu and Smalley (2000)], or the manufacturing procedure of device and composite through chemical treatment. Furthermore, the images of relevant defects were also detected and captured using various advanced measurement instruments. For example, Orlikowski, Nardelli, Bernholc and Roland (2000) studied the Stone-Wales defect in a CNT using an STM. Hashimoto, Suennaga, Gloter, Urita and Iijima (2004) explored the formation of the vacancy defects in a graphene layer using a high-resolution TEM. Besides, they have concluded that the defects in a CNT, such as topological defects or vacancy defects, tend to be numerous and stable under electron irradiation. The above literature has demonstrated the evidence of the existence of the structural defects in CNTs. Unfortunately, they were not taken into account in most of theoretical investigations, thus potentially leading to a large deviation from the experimental predictions.

Until recently, only a few studies have been done with regard to the effects of atomistic defects on the nanomechanical properties of CNTs. Hirai, Nishimaki, Mori, Kimoto, Akita, Nakayama and Tanaka (2003) investigated the influences of a pinhole defect on the yield strength and vibration properties of CNTs. Liew, He and Wong (2004) examined the elastic and plastic properties of MWCNTs under axial tension due to the formation of the Stone-Wales defects using MD simulation. Chandra, Namilae and Shet (2004) found that there are about 30-50% reduction in stiffness and Young's modulus due to the Stone-Wales defects through molecular static simulations using a conjugate gradient algorithm. Using quantum mechanical calculations and molecular mechanics simulation, Mielke, Troya, Zhang, Li, Xiao, Car, Ruoff, Schatz and Belytschko (2004) concluded that one-atom and two-atom vacancy defects would reduce the failure stresses by as much as 26%, and would also significantly lessen the failure strain. Tserpes, Papanikos and Tsirkas (2006) proposed an atomistic-based progressive fracture model to simulate the mechanical performance of CNTs with atomistic vacancy.

In this study, we aim at providing a systematic investigation on the role of atomistic defects in the nanomechanical properties and fracture behaviors of CNTs by using MD simulation. Not only the type of structural defects (namely the atomistic vacancy and the Stone-Wales defects) but also the defect number in percentage and the distribution pattern of the defects are addressed. Besides, the correlation between the fracture evolution of the CNTs with atomistic defects and the atomistic-level stress distribution is examined. Unlike the previous theoretical studies that

only take into account a small amount of atomistic vacancy, the considered defect rate in the present study is as much as about  $0.3 \text{ atom/nm}^2$ , i.e.,  $0.71\%$  atom amount, based on the estimation of Hashimoto, Suennaga, Gloter, Urita and Iijima (2004). The nanomechanical properties under investigation include the stress-strain curve, elastic modulus, ultimate strength and strain, and fracture evolution. To demonstrate the effectiveness of the MD simulation, the present results are compared with the theoretical/experimental data available in literature.

## 2 MD simulation

### 2.1 Tersoff-Brenner potential

Molecular dynamics (MD) is concerned with the simulation of particle dynamics based on the Newton's second law, where analytical or empirical potential functions are generally used to depict the atomistic interactions or bonding mechanisms in a molecular system. The formulation of MD is then defined by assessing the spatial gradient of the specified potential function. In literature, for covalent bond interactions such as carbon or silicon, several empirical potential functions have been introduced. In this study, the Tersoff-Brenner potential [Brenner (1990)] is adopted to model the covalent bonds between atoms in a CNT, in which the total covalent potential of a system  $E_{cov}$  is denoted as the sum of individual covalent bond energy:

$$E_{cov} = f_c(r_{ij}) \{V_R(r_{ij}) - b_{ij}V_A(r_{ij})\}, \quad (1)$$

where  $r_{ij}$  is the distance between two bonding atoms. In order to facilitate the computation of equilibrium of atoms, a specific cutoff function  $f_c(r_{ij})$  is implemented in the potential,

$$f_c(r_{ij}) = \begin{cases} 1 & (r_{ij} < R - D) \\ \frac{1}{2} - \frac{1}{2} \sin \left[ \frac{\pi}{2} (r_{ij} - R) / D \right] & (R - D < r_{ij} < R + D) \\ 0 & (r_{ij} > R + D) \end{cases} \quad (2)$$

Basically, the cutoff function varying from 0 to 1 is a simple decaying function that defines the weighting of covalent bonds within a certain distance. Furthermore,  $V_R(r_{ij})$  and  $V_A(r_{ij})$  in Eq. (1) represent the repulsive and attractive interactions, respectively. Those two parts of interactions are described in the following Morse-type potential:

$$V_R(r_{ij}) = \frac{D_e}{S-1} \exp\{-\beta\sqrt{2S}(r_{ij} - R_e)\}, \quad (3)$$

$$V_A(r_{ij}) = \frac{D_e S}{S-1} \exp\{-\beta \sqrt{2/S}(r_{ij} - R_e)\}, \quad (4)$$

where  $D_e$ ,  $S$ ,  $\beta$  and  $R_e$  are the coefficients of materials. Moreover,  $b_{ij}$  in Eq. (1) denotes the modification of the covalent bonding energy depending on  $\theta_{jik}$ , namely the bonding angle between two neighboring bonds. It is expressed as

$$b_{ij} = \left( 1 + a^n \left\{ \sum_{k(\neq i,j)} g(\theta_{jik}) \right\}^n \right)^{-\delta}, \quad (5)$$

$$g(\theta_{jik}) = 1 + c^2/d^2 - c^2/(d^2 + (h - \cos \theta_{jik})^2). \quad (6)$$

The coefficients used in the Tersoff-Brenner potential for carbon systems are listed in Tab. 1.

Table 1: The coefficients for Tersoff-Brenner potential for carbon

$R[\text{nm}]$	0.185
$D[\text{nm}]$	0.015
$De[\text{eV}]$	6.325
$S$	1.29
$\beta [A^{-1}]$	1.5
$Re[\text{nm}]$	0.1315
$a$	$1.1304 \times 10^{-2}$
$n$	1
$\delta$	0.80469
$c$	19
$d$	2.5
$h$	-1

## 2.2 Atomistic stress

In MD, the calculated results are all discrete, and thus, the Cauchy type of stress measure in continuum mechanics would no longer be applicable to the discrete atomic system. Shen and Atluri (2004b) addressed the issue by proposing a model transferring the discrete atomistic force field into an equivalent continuum system using the smoothed particle hydrodynamics (SPH) technique. In the model, the force density  $g(r)$  at point  $\mathbf{r}$  can be derived from the discrete atomistic force field by the SPH method:

$$g(r) = \sum_i f_i w(r - r_i, h), \quad (7)$$

where  $f_i$  is the force on atom  $i$ ,  $w(x, h)$  the smooth kernel function,  $h$  the smoothing length, and  $r_i$  the position of atom  $i$ . The following Gaussian function is chosen as the smooth kernel function in the study,

$$w(x, h) = \frac{1}{(\sqrt{\pi}h)^d} \exp\left(-\frac{x^2}{h^2}\right), \quad (8)$$

where  $d$  is the number of spatial dimensions. As  $h$  approaches to zero, the kernel function turns out to be a delta function. With an appropriately chosen  $h$ , the Gaussian kernel function would drop so rapidly that only a small number of particles would contribute to the force density. At last, the relationship between the atomistic force and stress fields can be obtained by analyzing the force state of the infinitesimal parallelepiped at point  $\mathbf{r}$ . With an appropriately defined smoothing length  $h$ , the Cauchy stress in the atomistic level at point  $\mathbf{r}$  falls into the following simple form:

$$\sigma(\mathbf{r}) = \frac{1}{2} \sum_i \sum_{j \neq i} r_{ij} \otimes f_{ij} \int_0^1 w[\mathbf{r} + (r_{ij}c - r_j)] dc. \quad (9)$$

### 2.3 Defects in CNT

Previous experimental measurements have shown that both vacancy defects and topological defects are commonly existed in CNTs. In the present study, two types of defects are considered. The first one is a vacancy defect, achieved by removal of one or more atoms together with the associated bonds from a CNT. If only one atom is removed, it is defined as a monovacancy defect, while it is termed a divacancy defect if two adjacent atoms together with 5 covalent bonds are simultaneously knocked off from the CNT system. An example of a CNT structure with a monovacancy defect is shown in Fig. 1(a). As seen in the figure, the center atom (atom 1) as well as the three neighboring bonds is simultaneously removed from the CNT to form the vacancy defect. The other is the Stone-Wales defect, a crystallographic defect, which occurs on carbon nanotubes as well as graphene, as shown in Fig. 1(b). Essentially, the Stone-Wales defect is a  $90^\circ$  rotation of two carbon atoms in a hexagonal network with respect to the midpoint of the bond, thus resulting in two pentagons and two heptagons. In general, it is formed under strain, and for undergoing the shear stress relaxation process in crystal, the atoms would move from one location to the other, thus changing the bond formation [see, e.g., Yakobson, Samsonidze, Samsonidze (2000)]. Unlike the vacancy defects, the Stone-Wales defects are created as a result of the translation of atoms and dislocation of bonds.

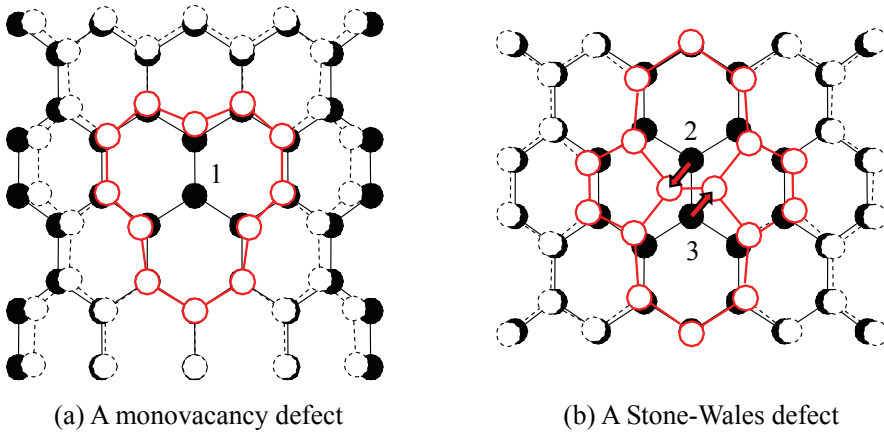


Figure 1: Formation of defects in CNT

### 3 Results

The effects of the atomistic defects on the nanomechanical properties of the SWCNTs are first investigated through MD simulation. Through a uniaxial tension test, the stress-strain relationship, elastic modulus, ultimate strength and strain, and fracture evolution are assessed. According to mechanics of materials, when a CNT is subjected to axial deformation, the resultant force  $F$  in the axial direction can be estimated by summing the interatomic forces of the atoms at the end side of the CNT. The associated axial stress  $\sigma$  can be then obtained by dividing the  $F$  by the cross-sectional area defined as  $A = C \times 0.34(\text{nm}^2)$ , where  $C$  is the circumference. On the other hand, the corresponding tensile strain can be computed by  $\varepsilon = (L - L_0)/L_0$ , in which  $L_0$  and  $L$  are the initial (undeformed) and elongated (deformed) length, respectively. From the stress-strain relationship, both the ultimate strength and strain can be extracted. Besides, from the slope of the stress-strain curve at an infinitesimal strain, the axial elastic modulus of the CNT can be also calculated. Finally, the fracture evolution of the defective CNTs under uniaxial tensile deformation can be also observed through the simulation.

### 3.1 Effect of defect rate of the atomistic vacancy

First of all, the effects of the defect rate on the nanomechanical properties of an armchair SWCNT are assessed. The radius of the SWCNT is 0.76 nm and the length is 11.99 nm. The vacancy defects are created on the armchair SWCNT by randomly knocking off certain atoms based on a specific defect amount. According to Hashimoto, Suennaga, Gloter, Urita and Iijima (2004), a rough estimation of the proportion of the defect in a graphene layer in practice is about 0.3 atom/nm<sup>2</sup>, equal to 0.71% atom amount. Therefore, the removal rates of atoms considered include 0.3%, 0.6%, 1.0%, and 2.0%. Fig. 2 shows the optimized configurations of a SWCNT with 0%, 0.3% and 2.0% defect rates at the free relaxation state, as well as the atomistic-level axial normal stress distributions. It is clear to find that the SWCNT with a 2.0% defect rate would undergo a significant flexural deformation. According to the stress distribution plots, both compressive and tensile stresses can be perceived in the defective SWCNT, where the compressive stress mostly takes place at the bottom (left) surface while the tensile at the top (right) surface of the SWCNT. Specifically, the maximum compressive stress takes place at the middle part of the bottom surface while the maximum tensile stress occurs in the vicinity of the defects on the top surface. Furthermore, by comparing with the defect-free SWCNT, the vacancy defects would induce stress concentration, and as a result, lead to a non-uniform stress distribution across the SWCNTs. The stress gradient becomes more considerable as the number of defects is larger. Note that the stress is considered as a preload for subsequent MD simulations.

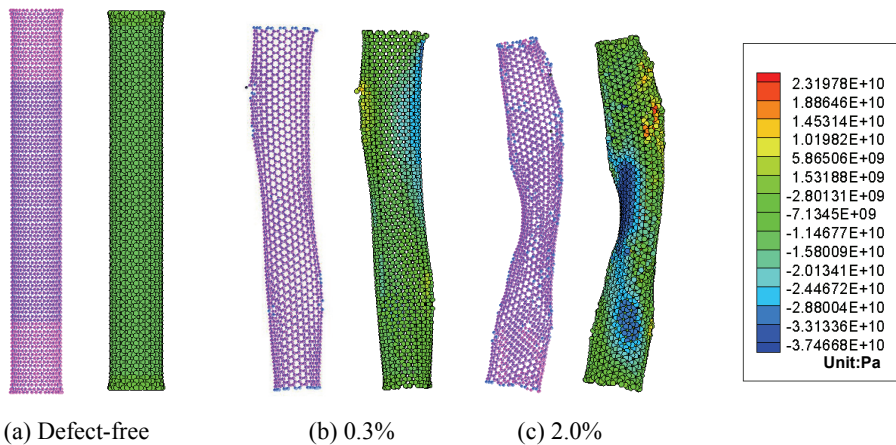


Figure 2: Optimized structures and associated stress fields at the free relaxation state under a different defect rate

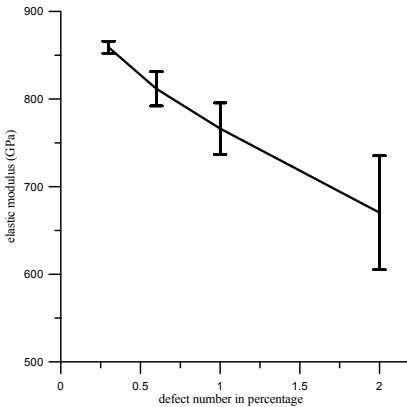


Figure 3: The elastic modulus at a different defect rate

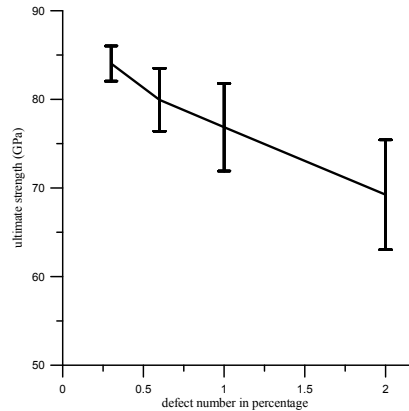


Figure 4: The ultimate strength at a different defect rate

To minimize the uncertainty when assessing the effects of defect rates, ten simulation trials are performed for each specific defect rate, each of which is associated with a random distribution pattern of the vacancy defects. The arithmetic mean value of these ten simulation results are presented, together with the associated standard deviation. The calculated elastic moduli under those defect rates are presented in Fig. 3. The results show that the average elastic moduli associated with 0.3%, 0.6%, 1.0%, and 2.0% defect rates are 859.0 GPa, 812.0 GPa, 766.0 GPa and 670.0 GPa. Evidently, the axial elastic modulus decreases with an increasing defect rate. In comparison with the elastic modulus of the defect-free SWCNT, i.e., about 900.0 GPa, the average decreases are about 4.56%, 9.78%, 14.89% and 25.56%, corresponding to the defect rates 0.3%, 0.6%, 1.0%, and 2.0%. The results are in a good agreement with those of Mielke, Troya, Zhang, Li, Xiao, Car, Ruoff, Schatz and Belytschko (2004) using molecular mechanics calculations. It should be noted that the standard deviation of the estimated elastic moduli tends to be larger for the SWCNTs with a higher defect rate. The ultimate strength versus the defect rate is illustrated in Fig. 4. The average ultimate strengths are 84.0 GPa, 80.0 GPa, 77.0 GPa and 69.0 GPa, corresponding to the defect rates. As compared to the defect-free SWCNT (i.e., 97 GPa), there are about 13.40%, 17.53%, 20.62% and 28.87% reduction for the defective ones, respectively. Similar to the aforementioned result trend of the elastic modulus, the standard deviation of these ultimate strengths also rises with the increase of the defect rate. The variation of the calculated results, i.e., the elastic modulus and ultimate strength, could be mainly attributed to the distribution of defects.

Furthermore, as shown in Fig. 5, the two SWCNTs consisting of an identical defect rate 2% have a different elastic modulus, i.e., 609 GPa and 733 GPa, respec-

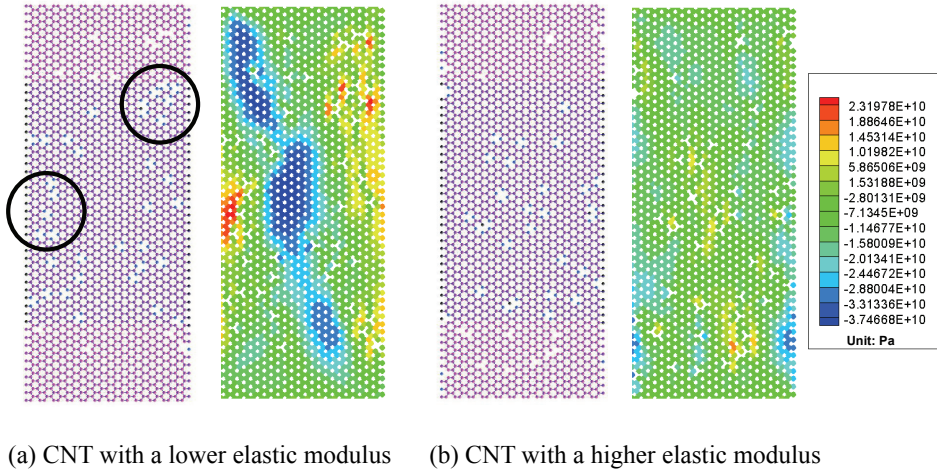


Figure 5: Stress fields of two armchair SWCNTs with an identical defect rate but a different defect layout

tively. It is found that there is a more significant aggregation of the created vacancy defects for the lower elastic modulus case, thus forming several more substantial stress-concentration portions and further causing the drop of the elastic modulus and ultimate strength. This again confirms that a higher defect rate would present a more wide-ranging defect distribution, and thus create a larger standard deviation in the calculated mechanical properties.

### 3.2 The Stone-Wales Defect

The effects of the Stone-Wales defect on the nanomechanical properties are addressed. Fig. 6 illustrates the stress-strain relationships for the armchair SWCNTs with a single Stone-Wales defect and a divacancy defect, respectively. It is shown that the ultimate strength and associated ultimate strain of the SWCNT with a single Stone-Wales defect are both larger than those with a single divacancy defect. In specific, the ultimate strength is 93 GPa and the associated strain is 0.37, which are 11% and 23% larger than those of the divacancy-defect case. This can be explained by that the Stone-Wales defect is formed simply through the so-called “pyracylene” transformation or atom rearrangement without removal of any atom or bond, thus retaining better integrity in atomistic structure and having a less impact on the mechanical properties. Moreover, a snapshot of the associated stress distributions at the free relaxation state is shown in Fig. 7, in which both compressive and tensile

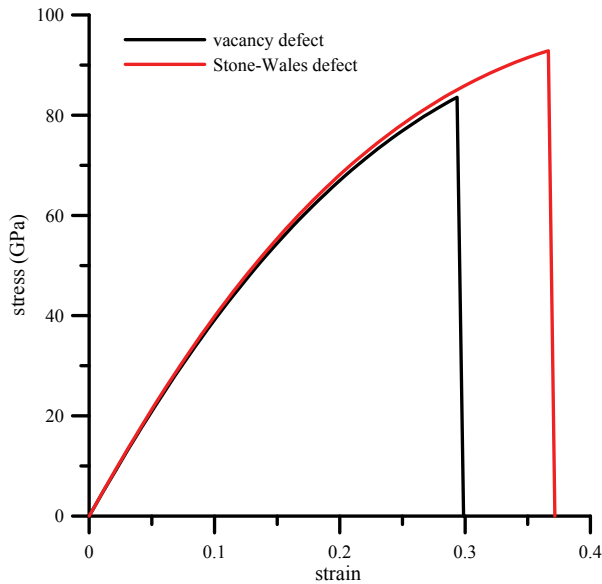


Figure 6: The stress-strain relationship for the defective armchair SWCNTs

stresses can be observed in these two defective SWCNTs. In addition, stress concentration occurs in the vicinity of the defects for both these two cases. However, a closer look at the stress distributions reveals that two high tensile stress bands are generated along  $\pm 45$  degree lines from the defect for the divacancy-defect case, and for the Stone-Wales-defect case, a high stress band along the 0 degree line is created.

### 3.3 Effect of the size of defective SWCNTs

The influences of the size of the armchair SWCNT with a divacancy defect on the nanomechanical properties are evaluated, where the defect is located at the middle of the SWCNTs. Fig. 8 shows the stress-strain curve of the SWCNTs with a different tube radius but of the same length 3.815 nm. Three tube radii are considered in the investigation, namely 0.766 nm, 1.534 nm, and 2.308 nm. As can be seen in the figure, the calculated ultimate strengths associated with these three defective SWCNTs are quite comparable, indicating that the tube radius would have a little effect on the ultimate strength of the defective SWCNTs. Relatively, it presents a much larger impact on the associated ultimate strain, where it is 0.299, 0.284 and 0.268 corresponding these three defective SWCNTs. In other words, the ultimate strain decreases with an increasing tube radius. However, according to

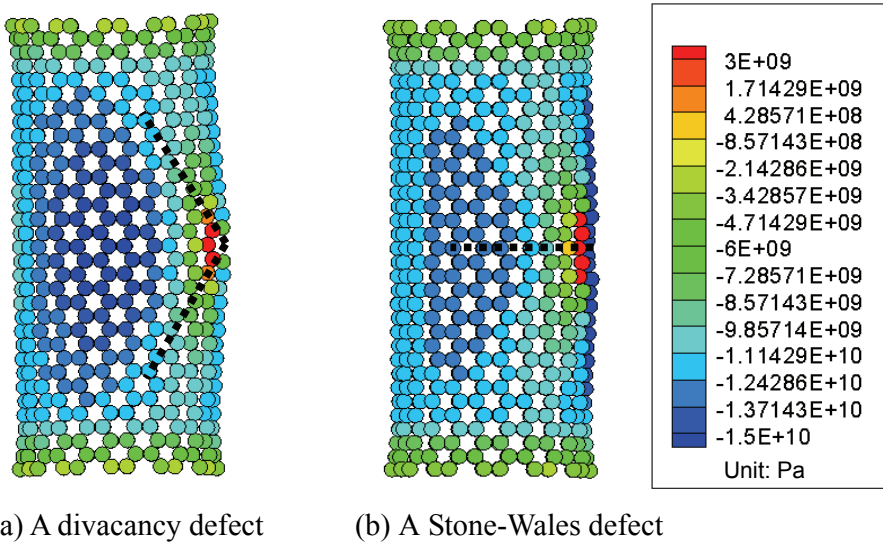


Figure 7: The axial normal stress distributions for the defective armchair SWCNTs at the free relaxation state

the slope of the stress-strain curves, the defective armchair SWCNT with a larger radius possesses a larger elastic modulus. The result is in a good agreement with the literature data of the defect-free cases, including Lu (1997) using an empirical model, Li and Chou (2003) using a molecular structural mechanics approach, and Chen, Cheng and Hsu (2007) using MD simulation. On the other hand, as shown in Fig. 9, the length of the defective armchair SWCNT shows an inconsiderable impact on the elastic modulus, ultimate strength and ultimate strain as it varies from 3.815 nm to 11.991 nm. The effect of the length is apparently not as significant as that of the tube radius.

### 3.4 Evolution of Fracture

The fracture evolutions of the armchair SWCNTs with one or three divacancy defects and one Stone-Wales defect, respectively, are presented, together with the atomistic-level stress distribution calculated based on Eq. (9). It is found that the SWCNTs with or without defects would show a sudden failure failure once the strain attains a critical value (i.e., the ultimate strain), at which the associated stress exhibits an abrupt drop down to zero. This concludes that the SWCNTs tend to be very brittle as the strain reaches the ultimate value. The observation is rather consistent with that of Yu, Lourie, Dyer, Moloni, Kelly and Ruoff (2000); Belytschko,

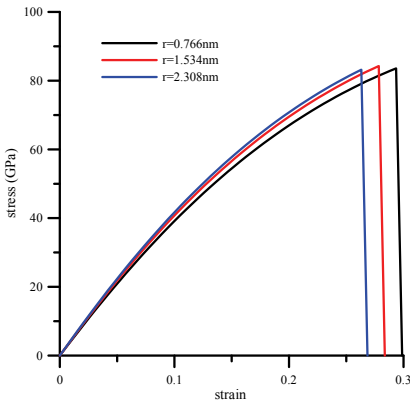


Figure 8: The stress-strain relationship of the armchair SWCNTs with a divacancy defect at a different tube radius

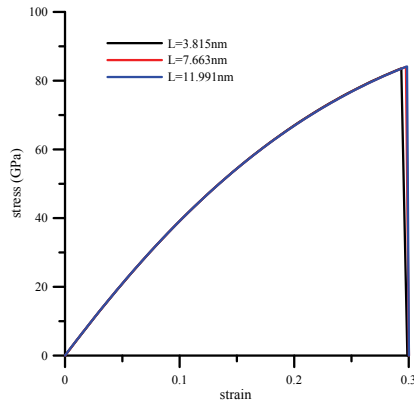


Figure 9: The stress-strain relationship of the armchair SWCNTs with a divacancy defect at a different tube length

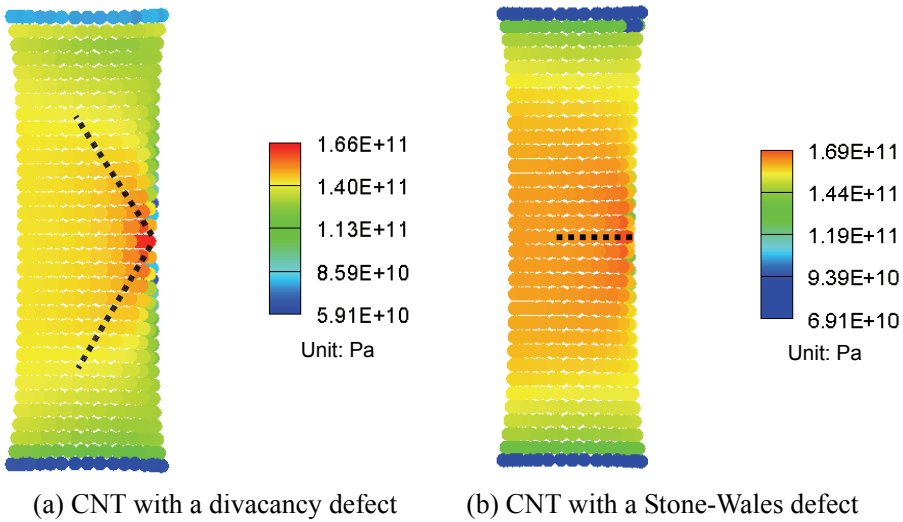


Figure 10: A snapshot of the stress distribution of the defective armchair SWCNTs before the onset of crack propagation.

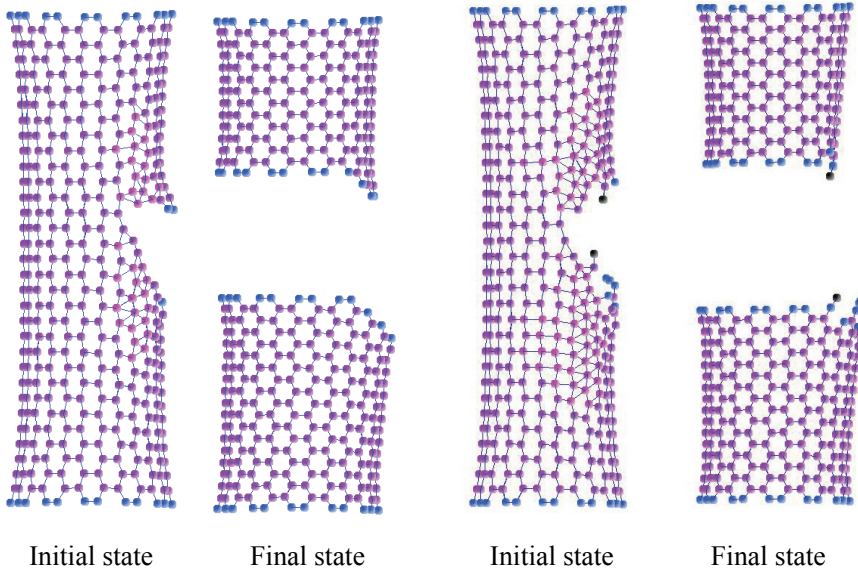
Xiao, Schatz and Ruoff (2002); and Tserpes, Papanikos and Tsirkas (2006), regardless of with or without atomistic defects.

The fracture evolutions associated with the SWCNT with a single divacancy defect

and that with a single Stone-Wales defect, residing in the middle of the tube, are shown in Fig. 11. Note that the stress distributions of these two defective SWCNTs at the free relaxation state have been previously shown in Fig. 7. A snapshot of the corresponding atomistic-level stress distributions right before the onset of crack propagation is shown in Fig. 10. Unlike the stresses at the free relaxation state, only tensile stresses can be detected in the two defective SWCNTs. Both these two figures show that there occurs a high stress concentration nearby the defects. Furthermore, there are also high stress zones at  $\pm 45$  degree lines from the defect for the divacancy case, and at a 0 degree line for the Stone-Wales-defect case immediately before the onset of crack propagation. The results agree well with those at the free relaxation state, as shown in Fig. 7.

The associated fracture evolutions are shown in Fig. 11. It turns out that these two types of atomistic defects would yield a different crack propagation path even though they have an identical defect rate and location. According to the fraction evolutions, the crack would initiate from the atomistic defect and then tend to quickly propagate in the direction of the high tensile stress concentration areas. In specific, for the SWCNT with a divacancy defect, the crack would start to propagate along the 45 degree line from the crack and then turn into the 0 degree line because of the rearrangement of atom positions, causing the redistribution of the atomistic stress. On the other hand, for the SWCNT with a Stone-Wales defect, the crack propagation direction also conforms to its high tensile stress concentration region, i.e., along the direction of the 0 degree line. Besides, the crack propagation would continue once initiated till a full fracture occurs. This indicates that SWCNTs are a very brittle material, and thus, would undergo a brittle fracture as the strain reaches the ultimate value, i.e., 0.3 for the vacancy-defect case and 0.37 for the Stone-Wales-defect case.

It should be, however, further noted that fracture evolution may strongly depend on other essential factors, namely the location, distribution pattern and number of the atomistic defects. As shown in Fig. 12, besides the divacancy defect residing at the middle of the SWCNT, two additional divacancy defects are created in between the first defect and the top end of the SWCNT. The corresponding atomistic-level stress distribution prior to the onset of crack propagation is also shown in Fig. 12. Evidently, high stress concentration also takes place nearby the newly additional divacancy defects, and more importantly, a high stress band is created along the direction between the first and the newly additional divacancy defects. The associated fracture evolution is shown in Fig. 13. As can be seen in the figure, the crack occurs almost simultaneously from these three divacancy defects, and then quickly propagates toward each other, and eventually tears off the entire SWCNT as the strain reaches a critical value.



(a) CNT with a divacancy defect      (b) CNT with a Stone-Wales defect

Figure 11: Predicted fracture evolutions of the defective armchair SWCNTs

#### 4 Conclusion

In this study, a systematic investigation of the influences of the atomistic defects in SWCNTs on their nanomechanical properties is performed through MD simulation. Furthermore, a study of the correlation between the fracture evolution and the local stress distribution is also performed. Parameters and factors such as the number, type (namely the vacancy and Stone-Wales defects), location and distribution pattern of defects are extensively examined. Some of the calculated results are extensively confirmed by the published experimental and theoretical data.

Some concluding remarks are drawn in the following:

1. At the free relaxation state, the optimal structure of the defective SWCNT is strongly dependent on the defect rate, where a higher defect rate would induce a more significant flexural deformation.
2. The average axial elastic modulus and ultimate strength of the defective SWCNTs decrease with an increasing defect rate. In comparison with the defect-free SWCNT, there are, respectively, about 4.56-25.56% and 13.40-

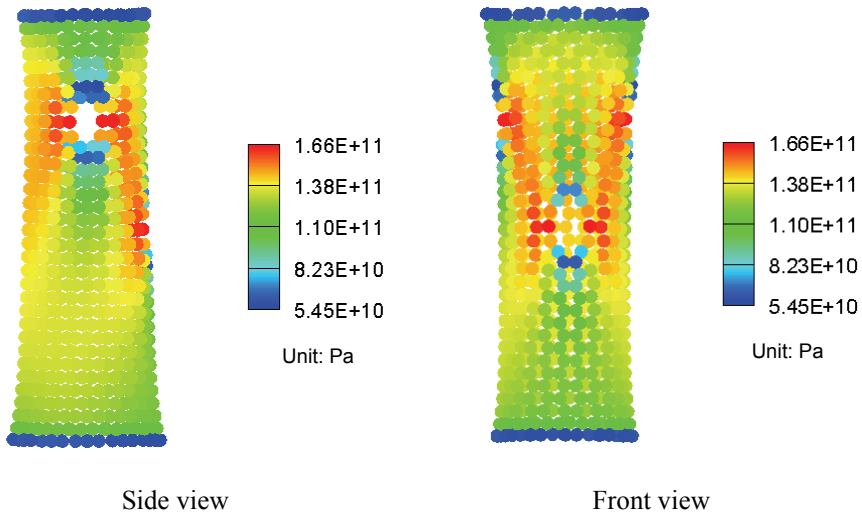


Figure 12: A snapshot of the atomistic-level stress distribution of the SWCNT with three divacancy defects before the onset of crack propagation.

28.87% drops in the axial elastic modulus and ultimate strength corresponding to 0.3-2.0% defect percentages.

3. It also turns out that the nanomechanical properties of the SWCNTs are considerably affected by not only the defect rate but also its distribution pattern.
4. The Stone-Wales defect has a less impact on the nanomechanical properties of the SWCNTs than the divacancy defect. Specifically, the ultimate strength and ultimate strain of the SWCNT with a single Stone-Wales defect are about 11% and 23% larger than those of the divacancy defect.
5. The stress calculations show that there is a high stress concentration around the atomistic defects of the SWCNTs at the free relaxation state and before or during the crack propagation under stain, where, in specific, two high tensile stress bands are created along  $\pm 45$  degree lines from the defect for the divacancy-defect case, and a high stress band is created along the 0 degree line for the Stone-Wales-defect case.
6. The tube radius of the defective SWCNTs would have a little effect on their ultimate strength as it varies from 0.766 nm to 2.308 nm, but show a relatively larger impact on the associated ultimate strain and tensile axial elastic

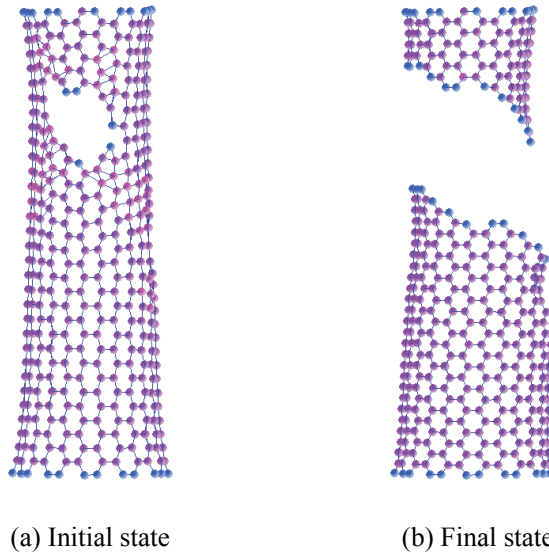


Figure 13: Predicted fracture evolution of the armchair SWCNT with three divacancy defects

modulus, where the former decreases and the latter increases with an increasing tube radius. On the other hand, the length of the SWCNTs has a trivial influence on the mechanical properties.

7. According to the fraction evolutions, it is found that the SWCNTs tend to be very brittle as the strain reaches the ultimate value.
8. The crack propagation process corresponds qualitatively and extensively to the local stress distribution, where the crack would initiate from the atomistic defect and then tend to quickly propagate in the direction of the high tensile stress concentration areas

In summary, the above results show that the structural defects are likely one of the main causes of the large variation in some reported nanomechanical properties of SWCNTs between the theoretical predictions and experimental measurements, or even among various experiments.

## Reference

**Andrews, R.; Jacques, D.; Qian, D.; Dickey, E. C. (2001):** Purification and structural annealing of multiwalled carbon nanotubes at graphitization temperatures.

*Carbon*, vol. 39, pp. 1681-1687.

**Belytschko, T.; Xiao, S. P.; Schatz, G. C.; Ruoff, R. S.** (2002): Atomistic simulations of nanotube fracture. *Physical Review B*, vol. 65, pp. 235430.

**Brenner, D. W.** (1990): Empirical potential for hydrocarbons for use in simulating the chemical vapor deposition of diamond films. *Physical Review B*, vol. 42, pp. 9458-9471.

**Chakrabarty, A.; Cagin, T.** (2008): Computational studies on mechanical and thermal properties of carbon nanotube based nanostructures. *CMC: Computers, Materials & Continua*, vol. 7, No. 3, pp. 167-190.

**Chandra, N.; Namilae, S.; Shet, C.** (2004): Local elastic properties of carbon nanotubes in the presence of Stone-Wales defects. *Physical Review B*, vol. 69, pp. 094101.

**Chen, W. H.; Cheng, H. C.; Hsu, Y. C.** (2007): Mechanical properties of carbon nanotubes using molecular dynamics simulations with the inlayer van der Waals interactions. *CMES: Computer Modeling in Engineering and Sciences*, vol. 20, pp. 123-145.

**Demczyk, B. G.; Wang, Y.M.; Cumings, J.; Hetman, M.; Han, W.; Zettl, A.; Ritchie, R.O.** (2002): Direct mechanical measurement of the tensile strength and elastic modulus of multiwalled carbon nanotubes. *Materials Science and Engineering A*, vol. 334, pp.173–178.

**Ebbesen, T. W.; Takada, T.** (1995): Topological and  $sp^3$  defect structures in nanotubes. *Carbon*, vol. 33, pp. 937-978.

**Ghanbari, J.; Naghdabadi, R.** (2009): Multiscale Nonlinear Constitutive Modeling of Carbon Nanostructures Based on Interatomic Potentials. *CMC: Computers, Materials & Continua*, vol. 10, No. 1, pp. 41-64.

**Hahn, J. R.; Kang, H.; Song, S.; Jeon, I. C.** (1996): Observation of charge enhancement induced by graphite atomic vacancy: A comparative STM and AFM study. *Physical Review B*, vol. 53, pp. R1725-R1728.

**Hashimoto, A.; Suennaga, K.; Gloter, A.; Urita, K.; Iijima, S.** (2004): Direct evidence for atomic defects in graphene layers. *Nature*, vol. 430, pp. 870-873.

**Hernandez, E.; Goze, C.; Bernier, P.; Rubio, A.** (1998): Elastic properties of C and  $B_xC_yN_z$  composite nanotubes. *Physical Review Letters*, vol. 80, pp. 4502-4505.

**Hirai, Y.; Nishimaki, S.; Mori, H.; Kimoto, Y.; Akita, S.; Nakayama, Y.; Tanaka, Y.** (2003): Molecular dynamics studies on mechanical properties of carbon nanotubes with pinhole defects. *Japanese Journal of Applied Physics*, vol. 42, pp. 4120-4123.

**Li, C. Y.; Chou, T. W.** (2003): Elastic moduli of multi-walled carbon nanotubes and the effect of van der Waals forces. *Composite Science and Technology*, vol. 63, pp. 1517-1524.

**Liew, K. M.; He, X. Q.; Wong, C. H.** (2004): On the study of elastic and plastic properties of multi-walled carbon nanotubes under axial tension using molecular dynamics simulation. *Acta Materialia*, vol. 52, pp. 2521-2527.

**Lu, J. P.** (1997): Elastic properties of carbon nanotubes and nanoropes. *Physical Review Letters*, vol. 79, pp. 1297-1300.

**Mawhinney, D. B.; Naumenko, V.; Kuznetsova, A.; Yates Jr., J. T.; Liu, J.; Smalley, R. E.** (2000): Surface defect site density on single walled carbon nanotubes by titration. *Chemical Physics Letters*, vol. 324, pp. 213-216.

**Mielke, S. L.; Troya, D.; Zhang, S.; Li, J. L.; Xiao, S.; Car, R.; Ruoff, R. S.; Schatz, G. C.; Belytschko, T.** (2004): The role of vacancy defects and holes in the fracture of carbon nanotubes. *Chemical Physics Letters*, vol. 390, pp. 413-420.

**Orlikowski, D.; Nardelli, B.; Bernholc, J.; Roland, C.** (2000): Theoretical STM signatures and transport properties of native defects in carbon nanotubes. *Physical Review B*, vol. 61, pp. 14194-14203.

**Poncharal, P.; Wang, Z. L.; Ugarte, D.; de Heer Popov, W. A.** (1999): Electrostatic deflections and electromechanical resonances of carbon nanotubes. *Science*, vol. 283, pp. 1513-1516.

**Salvetat, J. P.; Briggs, G. A. D.; Bonard, J. M.; Bacsá, R. R.; Kulik, A. J.; Stockli, T.; Burnham, N. A.; Forro, L.** (1999): Elastic and shear moduli of single-walled carbon nanotube ropes. *Physical Review Letters*, vol. 82, pp. 944-947.

**Shen, S.; Atluri S. N.** (2004a): Computational nano-mechanics and multi-scale simulation. *CMC: Computers, Materials & Continua*, vol. 1, No. 1, pp. 59-90.

**Shen, S.; Atluri S. N.** (2004b): Atomic-level stress calculation and continuum-molecular system equivalence. *CMES: Computer Modeling in Engineering and Sciences*, vol. 6, pp. 91-104.

**Treacy, M. M. J.; Ebbesen, T. W.; Gibson, J. M.** (1996): Exceptionally high Young's modulus observed for individual carbon nanotubes. *Nature*, vol. 381, pp. 678-680.

**Tserpes, K. I.; Papanikos, P.; Tsirkas, S. A.** (2006): A progressive fracture model for carbon nanotubes. *Composites: Part B*, vol. 37, pp. 662-669.

**Xie, G. Q.; Han, X.; Long, S. Y.** (2007): Characteristic of waves in a multi-walled carbon nanotube. *CMC: Computers, Materials & Continua*, vol. 6, No. 1, pp. 1-12.

**Xie, G. Q.; Long, S. Y.** (2006): Elastic vibration behaviors of carbon nanotubes

based on micropolar mechanics. *CMC: Computers, Materials & Continua*, vol. 4, No. 1, pp. 11-20.

**Yakobson, B. I.; Samsonidze, G.; Samsonidze, G. G.** (2000): Atomistic theory of mechanical relaxation in fullerene nanotubes. *Carbon*, vol. 38, pp. 1675-1680.

**Yu, M.; Lourie, O.; Dyer, M.; Moloni, K.; Kelly, T.; Ruoff, R.** (2000): Strength and breaking mechanism of multiwalled carbon nanotubes under tensile load. *Science*, vol. 287, pp. 637-640.